

# Grasping Fragile Objects Using A Stress-Minimization Metric

Zherong Pan<sup>1</sup>, Xifeng Gao<sup>2</sup>, and Dinesh Manocha<sup>3</sup>

**Abstract**—We present a new method to generate optimal grasps for brittle and fragile objects using a novel stress-minimization (SM) metric. Our approach is designed for objects that are composed of homogeneous isotropic materials. Our SM metric measures the maximal resistible external wrenches that would not result in fractures in the target objects. In this paper, we propose methods to compute our new metric. We also use our SM metric to design optimal grasp planning algorithms. Finally, we compare the performance of our metric and conventional grasp metrics, including  $Q_1$ ,  $Q_\infty$ ,  $Q_{G11}$ ,  $Q_{MSV}$ ,  $Q_{VEW}$ . Our experiments show that our SM metric takes into account the material characteristics and object shapes to indicate the fragile regions, where prior methods may not work well. We also show that the computational cost of our SM metric is on par with prior methods. Finally, we show that grasp planners guided by our metric can lower the probability of breaking target objects.

## I. INTRODUCTION

Grasp quality metrics are scalar functions defined on the set of possible grasps, which is used to compare the quality of different grasps. The performance and properties of (asymptotically) optimal grasp planning algorithms depend heavily on the type of grasp quality metrics used. A summary of these metrics can be found in [25]. The usual requirements for high-quality grasps include force closure, small contact force magnitudes, the preference of normal forces over frictional forces, higher resilience to external wrenches, and force resilience along all directions. For example, the  $Q_1$ ,  $Q_\infty$  metrics [8] take all these factors into consideration, while  $Q_{VEW}$  [17] is direction-dependent. The choice of a metric is typically based on the requirements of an application, but may also affect the choice of the resulting grasp planning algorithm. For example, the  $Q_1$ ,  $Q_\infty$  metrics are submodular, which allow fast discrete grasp points selection [26]. The  $Q_1$  metric has an optimizable lower-bound, which allows an optimization-based grasp planning algorithm [7] to jointly search for grasp points and grasp poses.

However, all the metrics considered so far make a common assumption that the target object is rigid and stiff, and will not crack or break due to the forces exerted by the grasp. As a result, prior methods assume that the target object is a rigid body and all the forces and torques are applied on the center-of-mass, which greatly simplifies the computation and analysis of metrics. However, this assumption does not hold when a robot is grasping fragile or brittle objects, and certain weak locations on the objects should be avoided to prevent fractures. Grasping of fragile objects has been considered in prior works [22], [1], which attempt to avoid breaking objects by developing safe grippers. Our goal is complimentary, as

we want to formulate new grasp metrics that reduce the stresses in fragile objects.

**Main Results:** We present a novel stress-minimization metric that takes into account the probability of the target object being broken into pieces. Based on the theory of brittle fracture [10], we formulate the set of external wrenches that can be resisted without causing fractures in the object. Similar to the  $Q_1$  metric [8], our metric measures the maximal size of the sphere-shaped subset of resistible wrenches. We refer to this new metric as the stress-minimization (SM) metric  $Q_{SM}$ . We show that  $Q_{SM}$  can be computed efficiently using the boundary element method (BEM) [6], given a surface triangle mesh of the object and a set of contact points. The cost of computing  $Q_{SM}$  is similar to that of computing  $Q_1$ . Using a simple scenario, we also show that most previous grasp metrics, including  $Q_1$ ,  $Q_\infty$  [8],  $Q_{G11}$  [4],  $Q_{VEW}$  [17], and  $Q_{MSV}$  [4], do not reflect the probability of the target object being broken, while  $Q_{SM}$  does. Finally, we show that conventional optimization-based grasp planning algorithms [5], [26], [14] can be modified to search for globally optimal grasps by maximizing  $Q_{SM}$ . Based on our algorithm, we can compute optimal grasps for a row of complex, high-genus objects with the lowest probability of breaking them. Computing  $Q_{SM}$  takes 4 – 8s and finding optimal grasps under  $Q_{SM}$  takes 1 – 5hr on average using a global optimization algorithm [14] or less than 10min using a stochastic optimization algorithm [27].

## II. RELATED WORK

We review related work in grasp quality metrics, material and fracture modeling, and grasp planning.

**Grasp Quality Metrics:** Although some grasp planners only consider external wrenches along some certain directions [21], more pertinent characterization of a robust grasp requires resilience to external wrenches along all directions, which is known as force closure [23]. However, infinitely many grasps can have force closure and some of them are classified as good grasps based on different quality metrics [25]. Most of the metrics  $Q$  are designed such that  $Q > 0$  implies force closure. Closely related metrics to our  $Q_{SM}$  are  $Q_1$ ,  $Q_\infty$  [8], which measures the maximal radius of an origin-centered wrench-space sphere contained in the convex set of resistible wrenches under contact force magnitude constraints.

**Material and Fracture Modeling:** Real world solid objects may result in brittle or ductile fractures under external forces, depending on the underlying materials. However, modeling the physics during fractures is difficult because they can undergo large deformations during fractures [10]. Fortunately, for grasp planning, we do not need to model these deformations precisely, but only need to detect where fractures might occur. In this case, the theory of linear elasticity suffices [10] and the stress induced by external wrenches

<sup>1</sup>Zherong is with Department of Computer Science, University of North Carolina at Chapel Hill. {zherong@cs.unc.edu} <sup>2</sup>Xifeng Gao is with Department of Computer Science, Florida State University. {gao@cs.fsu.edu} <sup>3</sup>Dinesh Manocha is with Department of Computer Science and Electrical & Computer Engineering, University of Maryland at College Park. {dm@cs.umd.edu}

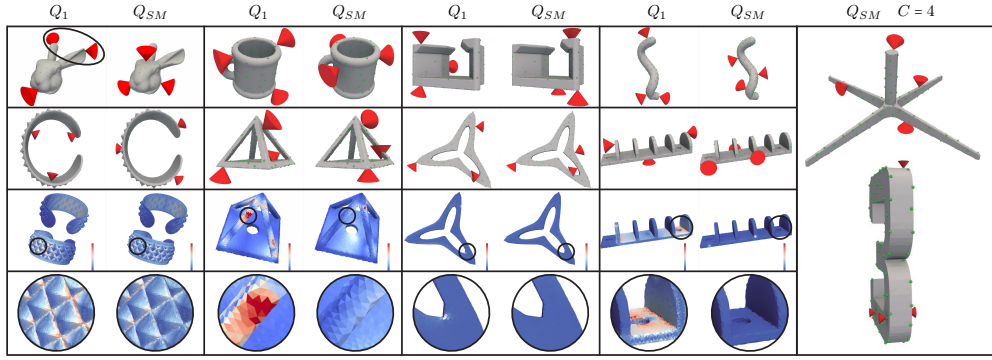


Fig. 1: First and second rows: We show globally optimal grasps for 8 different target objects based on  $Q_1$  (left) and  $Q_{SM}$  (right) in each box. These grasps are generated by choosing  $C = 3$  contact points (frictional cones in red) from  $N = 100$  potential contact points using BB, which takes 1.7hr to compute. The optimal grasp for the bunny head avoids the ears of the bunny under the  $Q_{SM}$  metric (black circle). Third and fourth rows: We plot the maximal stress configuration (color coded). Using  $Q_{SM}$  can drastically reduce the maximal stress as indicated in the black circle. Finally, we show two optimal grasps with  $C = 4$  and  $Q_{SM}$  on the right, which takes 5.4hr to compute.

on target objects can be computed efficient using the finite element method (FEM) [16] or the boundary element method (BEM) [6]. We use BEM as our computational tool because it can take the materials of the target object into consideration while only requires a surface triangle mesh, which is more amenable to robot grasp applications.

**Grasp Planning:** Given a grasp quality metric, an (asymptotically) optimal grasp planning algorithm finds a grasp that maximizes the grasp quality metric. Early algorithms [27] use sampling-based methods for planning. These algorithms are very general and they are agnostic to grasp quality metric types. However, more efficient algorithms such as [7], [26] can be designed if quality metrics have certain properties such as monotonicity and submodularity. A good grasp metric can also be used in learning based grasp planners such as [19], [18], [20] that use precomputed metrics to train a grasp quality function represented by a deep neural network and then use the function as a guidance.

### III. PROBLEM STATEMENT

In this section, we formulate the problem of stress-minimization grasp planning. Throughout the paper, we assume that the 3D target object is in its reference space, where the origin coincides with its center-of-mass. The object takes up a volume that is a closed subset  $\Omega \subset R^3$ . In addition, the object is under an external 6D wrench  $\mathbf{w}$  and a set of  $N$  external contact forces  $\mathbf{f}_1, \dots, \mathbf{f}_N$  at contact points  $\mathbf{x}_1, \dots, \mathbf{x}_N$  with unit contact normals  $\mathbf{n}_1, \dots, \mathbf{n}_N$ . If a grasp is valid, we have the following wrench balance condition:

$$\mathbf{w} = - \sum_{i=1}^N \begin{pmatrix} \mathbf{f}_i \\ \mathbf{x}_i \times \mathbf{f}_i \end{pmatrix} \quad \text{s.t.} \quad \|(\mathbf{I} - \mathbf{n}_i \mathbf{n}_i^T) \mathbf{f}_i\| \leq \theta \mathbf{n}_i^T \mathbf{f}_i, \quad (1)$$

where  $\theta$  is the frictional coefficient. A well-known method for comparing the quality of two different grasps is to compare their  $Q_1$  metric [8], which is the maximal radius of the origin-centered inscribed sphere in the convex hull of all possible resistible external wrenches when the magnitude of  $\mathbf{f}_i$  is bounded. Mathematically, this can be expressed as:

$$Q_1 = \max_r \quad \text{s.t.} \{ \mathbf{w} | \mathbf{w}^T \mathbb{W} \mathbf{w} \leq r^2 \} \subseteq \{ \mathbf{w} | \exists \mathbf{f}_1, \dots, \mathbf{f}_N, \text{ s.t. Equation (1), } \sum_{i=1}^N \mathbf{n}_i^T \mathbf{f}_i \leq 1 \},$$

where  $\mathbb{W}$  is the  $6 \times 6$  positive semi-definite metric tensor in the wrench space.

However, the formulation of  $Q_1$  metric assumes that the object remains rigid and will never be broken or decomposed into parts, no matter how large the external forces are. To relax this condition, we have to make use of the numerical models of brittle fracture, e.g., [10]. In these formulations, we assume that the object is made of homogeneous isotropic elastic material with  $\lambda, \mu$  being its Lamé material parameters [10]. This material model covers most target objects encountered in our daily lives, including objects made of copper, rubber, glass, and porcelain. When under external force fields  $\mathbf{g}(\mathbf{x}) : R^3 \rightarrow R^3$ , an infinitesimal displacement  $\mathbf{u}(\mathbf{x}) : R^3 \rightarrow R^3$  and a stress field  $\boldsymbol{\sigma}(\mathbf{x}) : R^3 \rightarrow R^{3 \times 3}$  will occur  $\forall \mathbf{x} \in \Omega$ .  $\mathbf{u}(\mathbf{x}), \boldsymbol{\sigma}(\mathbf{x})$  can be computed from  $\mathbf{g}(\mathbf{x})$  using the force balance condition:

$$\begin{aligned} \forall \mathbf{x} \in \Omega : \quad \boldsymbol{\epsilon} &\triangleq (\nabla \mathbf{u} + \nabla \mathbf{u}^T)/2 \\ \boldsymbol{\sigma} &\triangleq 2\mu \boldsymbol{\epsilon} + \lambda \text{tr}(\boldsymbol{\epsilon}) \mathbf{I} \\ \nabla \cdot \boldsymbol{\sigma} + \mathbf{g} &= 0 \end{aligned} \quad (2)$$

$$\forall \mathbf{x} \in \partial\Omega : \quad \mathbf{n}(\mathbf{x}) \cdot \boldsymbol{\sigma} + \sum_{i=1}^N \delta(\mathbf{x} - \mathbf{x}_i) \mathbf{f}_i = 0,$$

where we assume the boundary of  $\Omega$  is smooth almost everywhere with the unit outward normal defined as  $\mathbf{n}(\mathbf{x})$  and  $\delta$  is the Dirac's delta operator. Classical theory of brittle fracture [10] further assumes that there exists a tensile stress  $\sigma_{max}$  and brittle fractures will not happen if the following condition holds:

$$\forall \|\mathbf{d}\| = 1, \mathbf{x} \in \Omega : \quad \mathbf{d}^T \boldsymbol{\sigma}(\mathbf{x}) \mathbf{d} \leq \sigma_{max}.$$

In order to make sure that the grasp metric always takes bounded value, we propose to slightly modify the above condition and limit  $\boldsymbol{\sigma}(\mathbf{x})$  on both sides, leading to the following condition:

$$\forall \|\mathbf{d}\| = 1, \mathbf{x} \in \Omega : \quad -\sigma_{max} \leq \mathbf{d}^T \boldsymbol{\sigma}(\mathbf{x}) \mathbf{d} \leq \sigma_{max}. \quad (3)$$

Note that the stress tensor must be symmetric so that its singular values coincide with its eigenvalues. Given the theory of brittle fracture, the goal of our work is to propose a grasp metric  $Q_{SM}$  that measures grasp qualities with Equation (3) as a precondition, present algorithms to compute  $Q_{SM}$ , and analyze grasp planning algorithms that are based on our

$Q_{SM}$  metric.

#### IV. THE STRESS-MINIMIZATION METRIC $Q_{SM}$

Our construction of  $Q_{SM}$  is illustrated in Figure (2). The basic idea behind the construction of  $Q_{SM}$  is very similar to that of the  $Q_1$  metric. Intuitively, we first define a convex subset  $\mathbf{W}$  of the 6D wrench space, which contains resistible wrenches that does not violate Equation (3). We then define  $Q_{SM}$  as the maximal radius of the origin-centered sphere contained in  $\mathbf{W}$ .

##### A. Definition of $\mathbf{W}$ and $Q_{SM}$

Given a certain wrench  $\mathbf{w}$ , we need to determine whether  $\mathbf{w} \in \mathbf{W}$ . This can be performed by first computing  $\boldsymbol{\sigma}$  and then testing whether Equation (3) holds. However, Equation (2) is a relationship between  $\boldsymbol{\sigma}$  and  $\mathbf{g}(\mathbf{x})$  but not  $\mathbf{w}$ , so we need to find a relationship between  $\mathbf{g}$  and  $\mathbf{w}$ . In other words, we need to find a body force distribution such that the net effect of  $\mathbf{g}$  is equivalent to applying  $\mathbf{w}$  on the center-of-mass. Obviously, infinitely many formulations of  $\mathbf{g}$ s will satisfy this relationship and different choices of  $\mathbf{g}(\mathbf{x})$  will lead to different variants of  $Q_{SM}$  metrics. In this paper, we propose choosing  $\mathbf{g}$  as a linear function in  $\mathbf{x}$ . The most important reason behind this choice is that the computation of  $\boldsymbol{\sigma}$  can be performed using BEM [6] if  $\mathbf{g}$  is a harmonic function of  $\mathbf{x}$ , and BEM can be applied to a surface mesh representing the target object while FEM [16] requires a volume mesh. Under this choice, we have:  $\mathbf{g}(\mathbf{x}) = \mathbf{g}_0 + \nabla \mathbf{g} \mathbf{x}$ , where  $\mathbf{g}_0$  is the constant term, and  $\nabla \mathbf{g}$  is the constant spatial derivative tensor. Clearly  $\mathbf{g}(\mathbf{x})$  has 12 degrees of freedom (3 in  $\mathbf{g}_0$  and 9 in  $\nabla \mathbf{g}$ ) and we can solve for  $\mathbf{g}_0$  and  $\nabla \mathbf{g}$  to equate the effect of  $\mathbf{g}$  and  $\mathbf{w}$  as follows:

$$\mathbf{w} = \int_{\Omega} \begin{pmatrix} \mathbf{g} \\ \mathbf{x} \times \mathbf{g} \end{pmatrix} d\mathbf{x} = \begin{pmatrix} |\Omega| \mathbf{g}_0 \\ \mathcal{T} \begin{pmatrix} [\nabla \mathbf{g}]_x \\ [\nabla \mathbf{g}]_y \\ [\nabla \mathbf{g}]_z \end{pmatrix} \end{pmatrix},$$

where  $\mathcal{T} \triangleq \int_{\Omega} (\mathbf{x} \mathbf{x}^T, y \mathbf{x}^T, z \mathbf{x}^T) d\mathbf{x}$ . Also,  $[\nabla \mathbf{g}]_{x,y,z}$  are the first, second, and third column of  $\nabla \mathbf{g}$ , respectively. However, there are 9 degrees of freedom in  $\nabla \mathbf{g}$  but only 3 constraints so we have to solve for  $\nabla \mathbf{g}$  in a least square sense:

$$\nabla \mathbf{g} = \underset{\nabla \mathbf{g}}{\operatorname{argmin}} \int_{\Omega} \|\nabla \mathbf{g} \mathbf{x}\|^2 d\mathbf{x} \quad \text{s.t.} \quad \mathcal{T} \begin{pmatrix} [\nabla \mathbf{g}]_x \\ [\nabla \mathbf{g}]_y \\ [\nabla \mathbf{g}]_z \end{pmatrix} = \begin{pmatrix} \mathbf{w}_4 \\ \mathbf{w}_5 \\ \mathbf{w}_6 \end{pmatrix},$$

the solution of which can be computed analytically. In summary, we have:

$$\begin{pmatrix} \mathbf{g}_0 \\ [\nabla \mathbf{g}]_x \\ [\nabla \mathbf{g}]_y \\ [\nabla \mathbf{g}]_z \end{pmatrix} = \begin{pmatrix} \mathbf{I} \\ |\Omega| \end{pmatrix} \mathcal{M}^{-1} \mathcal{T}^T [\mathcal{T} \mathcal{M}^{-1} \mathcal{T}^T]^{-1} \mathbf{w}, \quad (4)$$

where  $\mathcal{M} \triangleq [\int_{\Omega} \mathbf{x} \mathbf{x}^T d\mathbf{x}] \otimes \mathbf{I}$  and  $\otimes$  denotes Kronecker product. The matrices  $\mathcal{T}, \mathcal{M}$  are constants and can be precomputed from the shape of the target object or, more specifically, from the inertia tensor. Given these definitions, we can now define  $\mathbf{W}$  as follows:

$$\mathbf{W} = \{\mathbf{w} | \exists \mathbf{g}, \mathbf{f}_1, \dots, \mathbf{f}_N, \mathbf{u}, \boldsymbol{\epsilon}, \boldsymbol{\sigma}, \text{ s.t. Equation (1), 2, 3, 4}\}. \quad (5)$$

Finally, we are ready to give a mathematical definition of  $Q_{SM}$  using the following optimization function:

$$Q_{SM} = \max r \quad \text{s.t.} \quad \{\mathbf{w} | \mathbf{w}^T \mathbb{W} \mathbf{w} \leq r^2\} \subseteq \mathbf{W}.$$

From the mathematical definition of  $Q_{SM}$ , we immediately have the following properties of  $\mathbf{W}$ :

**Lemma 4.1:**  $\mathbf{W}$  is a convex set.

*Proof:* Equation (1) is a set of quadratic cone constraints, which defines a convex set. Equation (2) is a set of infinite-dimensional linear constraints, which defines a convex set. Equation (3) is an infinite-dimensional PSD-cone constraint, which defines a convex set. Finally, Equation (4) is a linear constraint, which also defines a convex set. As the intersection of convex sets,  $\mathbf{W}$  is convex. ■

**Lemma 4.2:**  $\mathbf{W}$  is a compact set so that  $Q_{SM}$  is finite.

*Proof:* For any  $\mathbf{w} \neq 0$ ,  $\boldsymbol{\sigma}$  that satisfies all three conditions (Equation (1), Equation (2) and Equation (4)) cannot be zero for all  $\mathbf{x} \in \Omega$ , otherwise the last equation in Equation (2) will be violated. In other words, there exist  $\mathbf{d}$  and  $\mathbf{x}$  such that  $|\mathbf{d}^T \boldsymbol{\sigma}(\mathbf{x}) \mathbf{d}| > \epsilon > 0$ . If we multiply  $\mathbf{w}$  by  $\alpha > \sigma_{max}/\epsilon$ , Equation (3) will be violated so that  $\alpha \mathbf{w} \notin \mathbf{W}$ . Therefore,  $\mathbf{W}$  is bounded and is obviously closed, so that  $\mathbf{W}$  is compact and  $Q_{SM}$  is finite. ■

In addition, the following property of  $Q_{SM}$  is obvious:

**Lemma 4.3:**  $Q_{SM} > 0$  implies force closure.

The following property has been proved in [26] for  $Q_1$  and also holds for  $Q_{SM}$  by a similar argument:

**Lemma 4.4:**  $Q_{SM} = \min_{\mathbf{d}, \|\mathbf{d}\|=1} \max_{\mathbf{w} \in \sqrt{\mathbb{W}} \mathbf{W}} \mathbf{w}^T \mathbf{d}$ .

##### B. Discretization of $Q_{SM}$

The computation of an exact  $Q_{SM}$  is impractical because it involves infinite dimensional tensor fields:  $\boldsymbol{\sigma}, \boldsymbol{\epsilon}$ , so we have to discretize them using conventional techniques such as FEM [16] or BEM [6]. We provide the detailed derivation of BEM in [24] and summarize the main results here. Our BEM algorithm approximates the stress field  $\boldsymbol{\sigma}(\mathbf{x})$  to be piecewise constant on each triangular patch of the surface. Assuming that the target object has  $K$  surface triangles whose centroids are:  $\mathbf{x}_1, \dots, \mathbf{x}_K$ , we have  $K$  different stress values:

$$\begin{pmatrix} \sigma_x(\mathbf{x}_j) \\ \sigma_y(\mathbf{x}_j) \\ \sigma_z(\mathbf{x}_j) \end{pmatrix} = \mathcal{A}_j \begin{pmatrix} \mathbf{g}_0 \\ [\nabla \mathbf{g}]_x \\ [\nabla \mathbf{g}]_y \\ [\nabla \mathbf{g}]_z \end{pmatrix} + \mathcal{B}_j \begin{pmatrix} \mathbf{f}_1 \\ \vdots \\ \mathbf{f}_N \end{pmatrix} \quad \forall j = 1, \dots, K, \quad (6)$$

where  $\mathcal{A}, \mathcal{B}$  are dense coefficient matrices defined from BEM discretization and the detailed formulations are given in [24]. Note that computing the coefficients of these two matrices is computationally costly, for which a naive implementation of BEM requires  $\mathcal{O}(K^3)$  operations and acceleration techniques such as the H-matrix [13] can reduce this cost to  $\mathcal{O}(K \log^2 K)$  operations. However, these two matrices are constant and can be precomputed for a given target object shape, so the cost of BEM computation is not a part of grasp planning. After discretization, we arrive at the finite-dimensional version of the fracture condition:

$$\forall \|\mathbf{d}\| = 1, j = 1, \dots, K: -\sigma_{max} \leq \mathbf{d}^T \boldsymbol{\sigma}(\mathbf{x}_j) \mathbf{d} \leq \sigma_{max}. \quad (7)$$

The finite-dimensional version of  $\bar{\mathbf{W}}$ :

$$\bar{\mathbf{W}} \triangleq \{\mathbf{w} | \exists \mathbf{g}, \mathbf{f}_1, \dots, \mathbf{f}_N, \mathbf{u}, \boldsymbol{\epsilon}, \boldsymbol{\sigma}, \text{ s.t. Equation (1), 6, 7, 4}\},$$

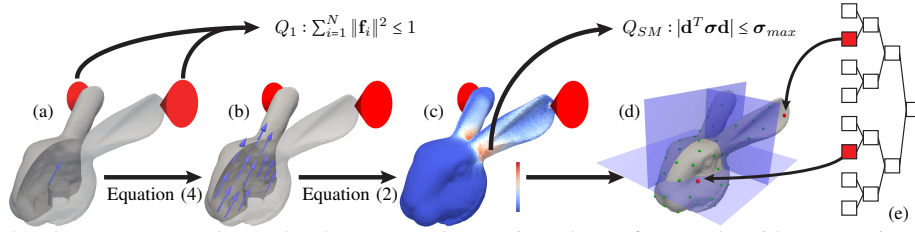


Fig. 2: A toy example where we grasp a bunny head represented as a triangular surface mesh, with grasp points on two ears (frictional cones in red). (a): When the bunny head is under an external wrench (blue arrow), the  $Q_1$  metric assumes that the wrench is applied on the center-of-mass. (b): Our  $Q_{SM}$  metric assumes that the external wrench is applied as a force field all over the volume of bunny head (blue arrows). (c): We use BEM to solve for a surface stress field (color coded on surface with high stress in red around connections between the ears and the head).  $Q_{SM}$  assumes that the stress along any direction  $\mathbf{d}$  is smaller than the tensile stress,  $\sigma_{max}$ . (d): When performing grasp planning, we first construct a KD-tree (transparent blue planes) for the set of  $N$  potential contact points. (e): We select  $C$  contact points (red points) by descending the tree.

and the finite-dimensional version of  $\bar{Q}_{SM}$  defined as:

$$\bar{Q}_{SM} = \text{argmax } r \quad \text{s.t. } \{\mathbf{w} | \mathbf{w}^T \mathbb{W} \mathbf{w} \leq r^2\} \subseteq \bar{\mathbf{W}}.$$

All the properties of the infinite-dimensional  $\mathbf{W}$  and  $Q_{SM}$  hold for the finite-dimensional version  $\bar{\mathbf{W}}$  and  $\bar{Q}_{SM}$  by a similar argument.

### C. Computation of $\bar{Q}_{SM}$

Computing  $\bar{Q}_{SM}$  amounts to a non-trivial global optimization. According to Lemma (4.4), the equivalent optimization problem for  $\bar{Q}_{SM}$  is:

$$\bar{Q}_{SM} = \min_{\mathbf{d}, \|\mathbf{d}\|=1} \max_{\mathbf{w} \in \sqrt{\mathbb{W}} \mathbf{W}} \mathbf{w}^T \mathbf{d},$$

for which direct optimization does not guarantee a global solution. In this section, we modify two existing algorithms to (approximately) compute  $\bar{Q}_{SM}$ , which were originally proposed to compute  $Q_1$ . In [26], the space of the unit vectors is discretized into a finite set of  $D$  directions:  $\mathbf{d}_1, \dots, \mathbf{d}_D$ . As a result, we can compute an upper bound for  $\bar{Q}_{SM}$  as:

$$\bar{Q}_{SM} \leq \min_{j=1, \dots, D} \max_{\mathbf{w} \in \sqrt{\mathbb{W}} \mathbf{W}} \mathbf{w}^T \mathbf{d}_j.$$

We can make this upper bound arbitrarily tight by increasing  $D$ . In another algorithm [28], a convex polytope  $\mathcal{C} \subseteq \bar{\mathbf{W}}$  is maintained using H-representation [12] and we can compute a lower bound for  $\bar{Q}_{SM}$  as:

$$\bar{Q}_{SM} \geq \min_{\mathbf{d}, \|\mathbf{d}\|=1} \max_{\mathbf{w} \in \sqrt{\mathbb{W}} \mathbf{C}} \mathbf{w}^T \mathbf{d}. \quad (8)$$

The global optimum of the optimization function in Equation (8) is easy to compute from an H-representation of  $\mathcal{C}$  by computing the distance between the origin and each face of  $\mathcal{C}$ . This lower bound can be iteratively tightened by first computing the blocking face normal  $\mathbf{d}$  of  $\mathcal{C}$  and then expanding  $\mathcal{C}$  via:

$$\mathcal{C} \leftarrow \text{ConvexHull}(\mathcal{C} \cup \{\text{argmax}_{\mathbf{w} \in \sqrt{\mathbb{W}} \mathbf{W}} \mathbf{w}^T \mathbf{d}\}).$$

These two algorithms can be implemented if we can find the supporting point of  $\sqrt{\mathbb{W}} \mathbf{W}$ , which amounts to the following conic programming problem:

$$\begin{aligned} & \text{argmax}_{\mathbf{w}, \mathbf{f}_i, \boldsymbol{\sigma}(\mathbf{x}_j)} \mathbf{w}^T \sqrt{\mathbb{W}} \mathbf{d} \\ & \text{s.t. Equation (1), 6, 4} \\ & \quad -\sigma_{max} \mathbf{I} \leq \boldsymbol{\sigma}(\mathbf{x}_j) \leq \sigma_{max} \mathbf{I} \quad \forall j = 1, \dots, K. \end{aligned} \quad (9)$$

The conic programming reformulation in Equation (9) can be solved using an interior point method [3]. Given this solution procedure, we summarize the modified version of [26] in Algorithm (1) and the modified version of [28] in

Algorithm (2). Note that Algorithm (2) is computationally costlier but it can approximate  $\bar{Q}_{SM}$  up to an arbitrary precision  $\epsilon$ , so we always use Algorithm (2) in the rest of the paper.

Compared with the  $Q_1$  metric, a major limitation of using the  $\bar{Q}_{SM}$  metric is that the computational cost is much higher. Note that the computational cost of solving Equation (9) is at least linear in  $K$  and can be superlinear depending on the type of conic programming solver used, such as [3]. This  $K$  is the number of surface triangles on the target object, which can be several thousands for complex objects. Fortunately, we can drastically reduce this cost by progressively adding constraints.

### D. Performance Optimization

The naive execution of Algorithm (2) can be prohibitively slow due to the repeatedly solving of Equation (9). The conic programming problem has  $K$  PSD-cone constraints with  $K$  being several thousands. Solving Equation (9) using interior point method [3] involves repeatedly solving a sparse linear system with a size proportional to  $K$ . We propose a method that can greatly improve the performance when solving Equation (9). Our idea is that when the global optimum of Equation (9) is reached, most PSD-cone constraints are inactive, so removing these constraints does not alter the solution. This idea is inspired by [29] which shows that, empirically, maximal stress only happens on a few sparse points on the surface of the target object. However, we do not know the active constraints as a prior. Therefore, we propose to progressively detect these active constraints.

In order to perform these computations, we first select a subset  $\mathbb{K} \subset \{1, \dots, K\}$  such that  $|\mathbb{K}| \ll K$  and  $\{\boldsymbol{\sigma}(\mathbf{x}_i) | i \in \mathbb{K}\}$  are the stress constraints that are most likely to be violated. In other words,  $\mathbb{K}$  is the initial guess of the active constraints. To select this set  $\mathbb{K}$ , we use a precomputation step and solve Equation (9) for 1000 times using random  $\mathbf{d}$  and record which PSD-cones are active. For each PSD-cone, we maintain how many times they become active during the 1000 solves of Equation (9). We then select the most frequent  $|\mathbb{K}|$  PSD-cones to form  $\mathbb{K}$ . After selecting  $\mathbb{K}$ , we maintain an active set  $\mathcal{S}$  that initializes to  $\mathbb{K}$  and we solve Equation (9) using constraints only in  $\mathcal{S}$ , which is denoted by:

$$\begin{aligned} & \text{argmax}_{\mathbf{w}, \mathbf{f}_i, \boldsymbol{\sigma}(\mathbf{x}_j)} \mathbf{w}^T \sqrt{\mathbb{W}} \mathbf{d} \\ & \text{s.t. Equation (1), 6, 4} \\ & \quad -\sigma_{max} \mathbf{I} \leq \boldsymbol{\sigma}(\mathbf{x}_j) \leq \sigma_{max} \mathbf{I} \quad \forall j \in \mathcal{S}. \end{aligned} \quad (10)$$

Equation (10) is convex and we can solve for its global optimum, after which we check the stresses on the remaining constraints and we pick the most violated constraint:

$$j^* = \underset{j \in \{1, \dots, K\}/\mathcal{S}}{\operatorname{argmax}} \sqrt{\|\sigma(\mathbf{x}_j)\sigma(\mathbf{x}_j)\|_2}. \quad (11)$$

If we have  $\sqrt{\|\sigma(\mathbf{x}_{j^*})\sigma(\mathbf{x}_{j^*})\|_2} < \sigma_{max}$ , then the global optimum of Equation (10) and Equation (9) will coincide. Otherwise, we add  $j^*$  to  $\mathcal{S}$ . This method is summarized in Algorithm (3) and is guaranteed to return the same global optimum of Equation (9). The complexity of Algorithm (3) is hard to analyze, but in practice it is orders of magnitude more efficient than considering all constraints at once.

## V. GRASP PLANNING UNDER THE SM METRIC

By grasp planning, our goal is to select  $C$  points that tend to maximize  $Q_{SM}$  given a set of  $N$  potential grasp points sampled on  $\partial\Omega$ . There are two types of algorithms that can be used for grasp planning, which are based on branch-and-bound (BB) [5], [26], [14] and sub-modular coverage (SMC) [26]. However, SMC requires the formulation in Equation (9) to be a sub-modular function in the set of contact points. Although this property holds for  $Q_1, Q_\infty$ , whether this property holds for  $Q_{SM}$  is still an open problem. However, we can use BB that only requires Equation (9) to be a monotonic function in the set of contact points, which is obvious. We follow [14] and build a KD-tree for the set of  $N$  potential grasp points, as illustrated in Figure (2)(d) and Figure (2)(e). We maintain a pointer to one KD-tree node for each of the  $C$  selected points. Next, we descend the tree until all the  $C$  pointers reach leaf nodes and keep track of the best set of  $C$  leaf nodes. BB can find the globally optimal set of  $C$  grasp points that maximize any monotonic grasp metric (see [14] for more details).

---

### Algorithm 1 A modified algorithm of [26] to compute $\bar{Q}_{SM}$

---

- 1: sample directions  $\mathbf{d}_{1, \dots, D}$  in  $\mathbf{SO}(3)$
  - 2: **for**  $i = 1, \dots, D$  **do**
  - 3:    $\triangleright$  Using Algorithm (3)
  - 4:   Solve Equation (9) with  $\mathbf{d} \leftarrow \mathbf{d}_i$  for  $\mathbf{w}_i$
  - 5: Return  $\min_i \{\mathbf{w}_i^T \sqrt{\mathbb{W}} \mathbf{d}_i\}$
- 

## VI. EVALUATIONS

We have implemented our algorithms for computing  $Q_{SM}$  and perform grasp planning using C++. The accuracy of BEM relies on the quality of the surface triangle mesh, so we first optimize the mesh quality to maximize the minimal internal angles of each surface mesh triangle using CGAL [2]. We implement the BEM using a kernel independent numerical integration scheme [9]. The most computationally costly step in BEM is the inversion of system matrices, for which we use LU-factorization accelerated by H-matrices [13]. Finally, we use CGAL [15] to construct convex hulls with exact arithmetic [11] to avoid degenerate cases. All the experiments are performed on a single desktop machine with two Xeon E5-2697 CPUs and 256Gb memory. In the rest of this section, we evaluate the properties of  $Q_{SM}$  and compare

---

### Algorithm 2 A modified algorithm of [28] to compute $\bar{Q}_{SM}$

---

- 1: sample initial directions  $\mathbf{d}_{1, \dots, D}$  in  $\mathbf{SO}(3)$
  - 2: **for**  $i = 1, \dots, D$  **do**
  - 3:    $\triangleright$  Using Algorithm (3)
  - 4:   Solve Equation (9) with  $\mathbf{d} \leftarrow \mathbf{d}_i$  for  $\mathbf{w}_i$ .
  - 5:  $\mathcal{C}_0 \leftarrow \text{ConvexHull}(\mathbf{w}_{1, \dots, D})$
  - 6: Solve Equation (8) with  $\mathcal{C} \leftarrow \mathcal{C}_0$  for  $\bar{Q}_{SM}^0$
  - 7: Store the blocking face normal on  $\mathcal{C}_0$  as  $\mathbf{d}_0$
  - 8: **while**  $k = 1, \dots$  **do**
  - 9:    $\triangleright$  Using Algorithm (3)
  - 10:   Solve Equation (9) with  $\mathbf{d} \leftarrow \mathbf{d}_{k-1}$  for  $\mathbf{w}_k$
  - 11:    $\mathcal{C}_k \leftarrow \text{ConvexHull}(\mathcal{C}_{k-1} \cup \{\mathbf{w}_k\})$
  - 12:   Solve Equation (8) with  $\mathcal{C} \leftarrow \mathcal{C}_k$  for  $\bar{Q}_{SM}^k$
  - 13:   Store the blocking face normal on  $\mathcal{C}_k$  as  $\mathbf{d}_k$
  - 14:   **If**  $|\bar{Q}_{SM}^k - \bar{Q}_{SM}^{k-1}| < \epsilon$  **then** return  $\bar{Q}_{SM}^k$
- 

it with other metrics, including  $Q_1, Q_\infty$  [8],  $Q_{G11}, Q_{MSV}$  [4], and  $Q_{VEW}$  [17].

---

### Algorithm 3 Progressive solve of Equation (9)

---

- 1:  $\mathcal{S} \leftarrow \mathbb{K}$
  - 2: **while**  $\mathcal{S} \neq \{1, \dots, K\}$  **do**
  - 3:   Solve Equation (10) for  $\mathbf{w}, \mathbf{f}_i, \sigma(\mathbf{x}_j)$
  - 4:   Pick  $j^*$  using Equation (11)
  - 5:   **if**  $\sqrt{\|\sigma(\mathbf{x}_{j^*})\sigma(\mathbf{x}_{j^*})\|_2} < 1$  **then**
  - 6:     Return  $\mathbf{w}, \mathbf{f}_i, \sigma(\mathbf{x}_j)$
  - 7:   **else**  $\mathcal{S} \leftarrow \mathcal{S} \cup \{j^*\}$
  - 8: Return  $\mathbf{w}, \mathbf{f}_i, \sigma(\mathbf{x}_j)$
- 

**Parameter Choices:** Computing  $Q_{SM}$  requires more parameters than are necessary for computing  $Q_1$ . Specifically, there are three additional variables: tensile stress  $\sigma_{max}$  and Lamé material parameters:  $\mu, \lambda$ . However, if we transform  $\mu, \lambda$  to an equivalent set of parameters: Young's modulus  $E$  and Poisson ratio  $\nu$  [16], it is obvious that  $Q_{SM}$  is proportional to  $\sigma_{max}$  and inversely proportional to  $E$ . Since the absolute value of a grasp metric is meaningless for grasp planning and only the relative value matters, we can always set  $\sigma_{max} = E = 1$  and choose only  $\nu$  according to the material type of the target object, and then set:

$$\mu = 1/2(1 + \nu) \quad \lambda = \nu / [(1 + \nu)(1 - 2\nu)].$$

In our experiments, we assume that objects are made of copper with  $\nu = 0.33$ . Finally, when running Algorithm (2), we set  $\epsilon = 0.001$ .

**Shape-Awareness:** The most remarkable advantage of  $Q_{SM}$  over previous metrics, such as  $Q_1, Q_\infty, Q_{MSV}, Q_{VEW}$ , and  $Q_{G11}$ , is shape awareness. In Figure (3)(a), our target object is a U-shaped tuning fork and we use a 3-point grasp. The shape of the tuning fork is asymmetric along the X-axis. According to Figure (3)(b), the best grasp under all metrics are the same, i.e., grasping the centroid point. However, previous metrics are not aware of the asymmetry, while  $Q_{SM}$  correctly reflects the fact that grasping the leftmost point is better than grasping the rightmost point



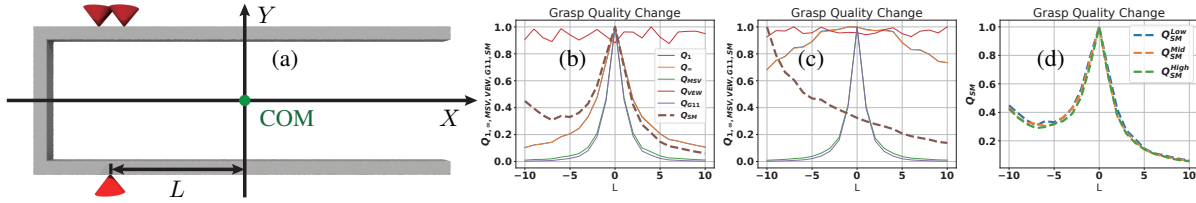


Fig. 3: (a): The target object is a U-shaped tuning fork. We test a 3-point grasp (frictional cones in red) where the distance to the center of mass (green) is  $L$ . (b): We plot the change of  $Q_1$ ,  $Q_\infty$ ,  $Q_{MSV}$ ,  $Q_{VEW}$ ,  $Q_{G11}$ , and  $Q_{SM}$  against  $L$  under 4 different conditions, where  $Q_{VEW}$  is not stable and  $Q_1$ ,  $Q_\infty$ ,  $Q_{MSV}$ ,  $Q_{G11}$  do not reflect asymmetric. Here, we apply equal weights to the forces and torques with  $\mathbb{W}_{bd} = \text{Id}$ . (c): We use lower weights for torques with  $\mathbb{W}_c = \text{diag}(1, 1, 1, 0.01, 0.01, 0.01)$ , in which case the best grasp under  $Q_{SM}$  is different from that under the four other metrics. (d): We plot  $Q_{SM}$  using  $\mathbb{W}_{bd}$  and meshes of different resolutions (Low:  $K = 5730$ , Mid:  $K = 24204$ , High:  $K = 94398$ ).

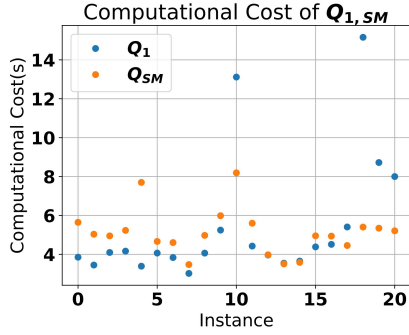


Fig. 4: We compare the computational cost of computing  $Q_1$  and  $Q_{SM}$  for 20 random target objects and grasps.

because it is less likely to break the object. If we change the metric  $\mathbb{W}$  and emphasize force resistance over torque resistance, then the difference between  $Q_{SM}$  and previous metrics is more visible and even the best grasp changes as shown in Figure (3)(c).

**Robustness to Mesh Resolution:** The change of  $Q_{SM}$  is not sensitive to the resolution of the surface meshes, as shown in Figure (3)(d), which makes  $Q_{SM}$  robust to target objects discretized using small, low-resolution meshes. As we increase  $K$  from 5730 to 24204 and finally to 94398, the change of  $Q_{SM}$  against  $L$  is almost intact, with very small fluctuations around  $L = -5$ .

**Computational Cost:**  $Q_{SM}$  has higher computational cost than  $Q_1$ . Most of the computational overhead lies in the assembly of matrices  $\mathcal{A}, \mathcal{B}$ , which involves the direct factorization of a large, dense matrix. However, this assembly is precomputation and is required only once for each target object before grasp planning. In Figure (3)(d), this step takes 112s when  $K = 5730$ , 1425s when  $K = 24204$ , and 3892s when  $K = 94398$ . After precomputation, the costs of evaluating  $Q_{SM}$  and  $Q_1$  are very similar, as shown in Figure (4). This implies that using  $Q_{SM}$  does not incur a higher cost in grasp planning. This is largely due to the progressive Algorithm (3), which greatly reduces the number of constraints in solving Equation (9). Without this method, solving Equation (9) is prohibitively costly as it requires the solve of a sparse linear system of a size proportional to  $K$ .

**Grasp Planning:** In Figure (1), we show globally optimal grasps for 8 different target objects under both the  $Q_{SM}$  and  $Q_1$  metric. To generate these results, we choose  $C = 3$  contact points from  $N = 100$  potential contact points using branch-and-bound. These contact points are generated using

Poisson disk sampling. The computational cost of BB, on average, is 1.7hr under  $Q_{SM}$  and 0.6hr under  $Q_1$ . When we choose  $C = 4$ , the average computational cost under  $Q_{SM}$  increases to 5.4hr. Although the cost of computing  $Q_{SM}$  is comparable to that of computing  $Q_1$ , we found that  $Q_{SM}$  tends to create more local minima so BB needs to create a larger search tree under  $Q_{SM}$ . In the third row of Figure (1), we show the maximal stress configuration in  $\mathbb{W}$  and the corresponding stress configuration under  $Q_1$  next to each other. The advantage of  $Q_{SM}$ , which suppresses the stress to resist the same external wrench, is quite clear. For some target objects, the high stress is concentrated in a very small region and we indicate these regions using black circles. Finally, for applications where globally optimal grasps are too costly to compute and only sub-optimal grasps are needed, users can choose stochastic grasp planning algorithms such as [27], which can return a sub-optimal grasp under  $Q_{SM}$  within 10min of computation.

## VII. CONCLUSION AND LIMITATION

We present the SM metric, which reflects the tendency of a target object to be broken during grasping. As a result, a grasp maximizing  $Q_{SM}$  will minimize the probability of breaking a fragile object. We show that  $Q_{SM}$  can be computed using previous methods and its computational cost can be drastically reduced by progressively detecting the active set. Finally, we show that grasp planning under  $Q_{SM}$  can be performed using BB algorithms. Our experiments show that  $Q_{SM}$  is aware of geometric fragility while  $Q_{1,\infty,MSV,VEW,G11}$  are not. We also show that using  $Q_{SM}$  does not increase the computational cost of the resulting grasp planning algorithm.

The major limitation of our work is that computing  $Q_{SM}$  requires a costly precomputation step to solve the BEM problem. In addition, the BEM problem requires high-quality, watertight surface meshes of target objects, while in many applications we only have objects represented using point clouds. An avenue of future research is to infer the value of  $Q_{SM}$  for given unknown objects using machine learning, as is done in [19]. Finally,  $Q_{SM}$  requires user to input the Poisson ratio, which is a material parameter. We are considering detecting these parameters from casual inputs such as RGBD images.

## ACKNOWLEDGEMENT

This work was supported in part by ARO Grants W911NF1910069, W911NF1910315, NSF-IIS-1910486, and Intel.

## REFERENCES

- [1] A. Al-Ibadi, S. Nefti-Meziani, and S. Davis, "Active soft end effectors for efficient grasping and safe handling," *IEEE Access*, vol. 6, pp. 23 591–23 601, 2018.
- [2] P. Alliez, C. Jamin, L. Rineau, S. Tayeb, J. Tournois, and M. Yvinec, "3D mesh generation," in *CGAL User and Reference Manual*. CGAL Editorial Board, 2019.
- [3] E. D. Andersen and K. D. Andersen, "The mosek interior point optimizer for linear programming: an implementation of the homogeneous algorithm," in *High performance optimization*. Springer, 2000, pp. 197–232.
- [4] Byoung-Ho Kim, Sang-Rok Oh, Byung-Ju Yi, and Il Hong Suh, "Optimal grasping based on non-dimensionalized performance indices," in *Proceedings 2001 IEEE/RSJ International Conference on Intelligent Robots and Systems. Expanding the Societal Role of Robotics in the Next Millennium (Cat. No.01CH37180)*, vol. 2, Oct 2001, pp. 949–956 vol.2.
- [5] J. Clausen, *Branch and Bound Algorithms-Principles and Examples*. Citeseer, 1999.
- [6] T. A. Cruse, D. Snow, and R. Wilson, "Numerical solutions in axisymmetric elasticity," *Computers & Structures*, vol. 7, no. 3, pp. 445–451, 1977.
- [7] H. Dai, A. Majumdar, and R. Tedrake, *Synthesis and Optimization of Force Closure Grasps via Sequential Semidefinite Programming*. Cham: Springer International Publishing, 2018, pp. 285–305.
- [8] C. Ferrari and J. Canny, "Planning optimal grasps," in *Proceedings 1992 IEEE International Conference on Robotics and Automation*, May 1992, pp. 2290–2295 vol.3.
- [9] P. Fiala and P. Rucz, "Nihu: An open source c++ bsm library," *Advances in Engineering Software*, vol. 75, pp. 101–112, 2014.
- [10] G. A. Francfort and J.-J. Marigo, "Revisiting brittle fracture as an energy minimization problem," *Journal of the Mechanics and Physics of Solids*, vol. 46, no. 8, pp. 1319–1342, 1998.
- [11] T. Granlund and G. D. Team, *GNU MP 6.0 Multiple Precision Arithmetic Library*. United Kingdom: Samurai Media Limited, 2015.
- [12] B. Grünbaum and G. C. Shephard, "Convex polytopes," *Bulletin of the London Mathematical Society*, vol. 1, no. 3, pp. 257–300, 1969.
- [13] W. Hackbusch, "A sparse matrix arithmetic based on h-matrices. part i: Introduction to h-matrices," *Computing*, vol. 62, no. 2, pp. 89–108, 1999.
- [14] K. Hang, J. A. Stork, N. S. Pollard, and D. Kragic, "A framework for optimal grasp contact planning," *IEEE Robotics and Automation Letters*, vol. 2, no. 2, pp. 704–711, April 2017.
- [15] S. Hert and M. Seel, "dD convex hulls and delaunay triangulations," in *CGAL User and Reference Manual*. CGAL Editorial Board, 2019.
- [16] T. J. Hughes, *The finite element method: linear static and dynamic finite element analysis*. Courier Corporation, 2012.
- [17] Z. Li and S. S. Sastry, "Task-oriented optimal grasping by multifingered robot hands," *IEEE Journal on Robotics and Automation*, vol. 4, no. 1, pp. 32–44, Feb 1988.
- [18] M. Liu, Z. Pan, K. Xu, K. Ganguly, and D. Manocha, "Generating grasp poses for a high-dof gripper using neural networks," *arXiv preprint arXiv:1903.00425*, 2019.
- [19] J. Mahler, J. Liang, S. Niyaz, M. Laskey, R. Doan, X. Liu, J. Aparicio, and K. Goldberg, "Dex-net 2.0: Deep learning to plan robust grasps with synthetic point clouds and analytic grasp metrics," in *Proceedings of Robotics: Science and Systems*, 07 2017.
- [20] J. Mahler, F. T. Pokorny, B. Hou, M. Roderick, M. Laskey, M. Aubry, K. Kohlhoff, T. Kröger, J. Kuffner, and K. Goldberg, "Dex-net 1.0: A cloud-based network of 3d objects for robust grasp planning using a multi-armed bandit model with correlated rewards," in *2016 IEEE International Conference on Robotics and Automation (ICRA)*. IEEE, 2016, pp. 1957–1964.
- [21] J. Mahler, F. T. Pokorny, Z. McCarthy, A. F. van der Stappen, and K. Goldberg, "Energy-bounded caging: Formal definition and 2-d energy lower bound algorithm based on weighted alpha shapes," *IEEE Robotics and Automation Letters*, vol. 1, no. 1, pp. 508–515, 2016.
- [22] B. Matulevich, G. E. Loeb, and J. A. Fishel, "Utility of contact detection reflexes in prosthetic hand control," in *2013 IEEE/RSJ International Conference on Intelligent Robots and Systems*, Nov 2013, pp. 4741–4746.
- [23] V. . Nguyen, "Constructing force-closure grasps," in *Proceedings. 1986 IEEE International Conference on Robotics and Automation*, vol. 3, April 1986, pp. 1368–1373.
- [24] Z. Pan, X. Gao, and D. Manocha, "Generating optimal grasps under a stress-minimizing metric," in *arXiv:1907.08749*, 2019.
- [25] M. A. Roa and R. Suárez, "Grasp quality measures: review and performance," *Autonomous robots*, vol. 38, no. 1, pp. 65–88, 2015.
- [26] J. D. Schulman, K. Goldberg, and P. Abbeel, "Grasping and fixturing as submodular coverage problems," in *Robotics Research*. Springer, 2017, pp. 571–583.
- [27] Z. Zhang, J. Gu, and J. Luo, "Evaluation of genetic algorithm on grasp planning optimization for 3d object: A comparison with simulated annealing algorithm," in *2013 IEEE International Symposium on Industrial Electronics*, May 2013, pp. 1–8.
- [28] Y. Zheng, "An efficient algorithm for a grasp quality measure," *IEEE Transactions on Robotics*, vol. 29, no. 2, pp. 579–585, 2012.
- [29] Q. Zhou, J. Panetta, and D. Zorin, "Worst-case structural analysis," *ACM Trans. Graph.*, vol. 32, no. 4, pp. 137:1–137:12, July 2013.